Materials Chemistry Horizons RESEARCH

Preparation of a New Magnetic Nanocomposite for the Removal of Dye Pollutions from Aqueous Solutions: Synthesis and Characterization

Ata Mehdizadeh[1], Peyman Najafi Moghadam[2]*,Sedigheh Ehsanimehr[2], Amir Reza Fareghi[2]

[1] Department of Applied Chemistry, Faculty of Chemistry, Urmia University, Urmia – Iran
[2] Department of Organic Chemistry, Faculty of Chemistry, Urmia University, Urmia – Iran

Corresponding author: p_najafi27@yahoo.com (P. Najafi Moghadam)

Mater. Chem. Horizons, 2022, 1(1), 23-34 10.22128/mch.2022.544.1003 OPEN ACCESS

ABSTRACT

In the present study, a new magnetic nanocomposite was synthesized with the capability to remove the dye pollutant from aqueous solutions. In the first step, magnetite nanoparticle was synthesized via the co-precipitation method and then, they were modified with 3-aminopropyltriethoxysilane (APTES) and acryloyl chloride, respectively. Then itaconic acid (IA) and 2-hydroxyethyl methacrylate were grafted on the modified nanoparticles via in *situ* copolymerization to prepare the final nanocomposite. The prepared nanocomposite was used as the adsorbent for the removal of the methylene blue as a typical dye from aqueous solutions. According to the obtained results, the nanocomposite showed high adsorption efficiency toward the methylene blue dye within 15 minutes and the other optimized values are pH=11, adsorbent dosage=30 mg, and initial concentration of the dye=20 ppm. Different parameters such as pH, amount of adsorbent, initial concentration of the dye, and contact time were investigated and optimized. Moreover, the synthesized nanocomposite was characterized by different methods such as FT-IR, VSM, TGA, XRD, and FE-SEM analyses. The result of VSM shows that the obtained nanocomposite has a magnetic property, which eases its separation and its amount, which is 31.72 emu.g^{-1}.

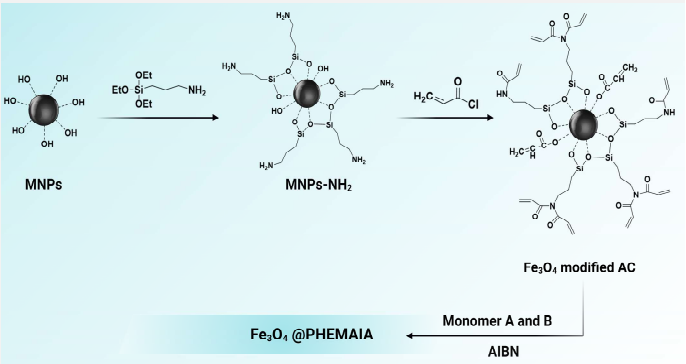

Keywords: Magnetic nanocomposite, methylene blue, dye removal, adsorption

1. Introduction

In recent years, the purification and removal of pollutants from water have been a necessary concern. Among water pollutants, industrial dyes waste is considerable and their improper discharge into the environment has irreparable effects on human health and other organisms. Industrial dyes waste is a mostly carcinogenic and direct effect on photosynthesis [1,2]. Moreover, they are stable compounds and resistant to biodegradation and oxidative agents [3,4].

Different methods have been used for the removal of dye pollutants from wastewater such as biological treatment [5], coagulation/flocculation [6], ozone treatment [7], chemical oxidation [8], membrane filtration [9], ion exchange [10], photocatalytic degradation [11], and adsorption [12]. Adsorption has been introduced as an effective and desirable method due to its high efficiency, ease of operation, and availability of various adsorbents. Different kinds of adsorbents have been used such as activated carbon (AC), agriculture wastes, silicate, clay, and solid wastes from industry [13, 14]. Recently, magnetic recyclable materials have been considered a smart and prominent scope for investigators [15, 16].

Several magnetic species are modified and used as magnetic carriers to manufacture all sorts of magnetic nanocomposites, such as γ-Fe_2O_3[17, 18], Fe_3O_4 [15, 19], and MFe_2O_4 (M=Ni, Co, Zn, and Cu)[20, 21]. Among these, the Fe_3O_4 nanoparticles (MNPs) as magnetic compounds have attracted a lot of attention due to their high surface area, ease of modification, and simplicity of separation [15, 22]. However, despite these advantages, the MNPs are

Received: May 22, 2022
Received in revised: June 13, 2022
Accepted: June 25, 2022

associated with deficiencies such as aggregation, oxidation in air, and instability under acidic conditions. To decrease the undesirable features, the bare MNPs should be embedded into a host matrix such as polymers [23]. The encapsulation of MNPs into polymer matrices prevents direct contact of the magnetic substance with the environment, improves their colloidal and chemical stability, and decreases toxicity [24].

Methylene blue (MB) is one of the most famous cationic dyes useful in the wool, silk, and cotton dyeing industries. It has a series of harmful side effects on the human body and animals such as eye irritation, vomiting, confusion, and sweating which requires the removal of dye before discharging to ambient waters [25-, 27].

In this work, a novel magnetic nano-adsorbent is synthesized by modification of bare Fe_3O_4. Then poly(2-hydroxyethyl methacrylate-*co*-itaconic acid) (PHEMA-IA) is grafted on modified Fe_3O_4 by in-situ copolymerization to synthesize the final nanocomposite. The synthesized nanocomposite is used as an adsorbent to remove the MB dye from aqueous solutions. Various characterization methods are employed to analyze the structure of the synthesized materials. In addition, the different adsorption parameters such as pH, adsorbent dosage, initial concentration of the dye, and contact time are investigated and optimized. Moreover, the adsorption isotherms and kinetic models are studied.

2. Experimental

2.1. Materials

2-Hydroxyethyl methacrylate (HEMA) (>97% Merck) was distilled under reduced pressure before use. Acryloyl chloride (AC) (>96% Merck) was also distilled under an inert atmosphere before use. AIBN (%98 Merck) was recrystallized from hot methanol and kept away from light. Other chemicals and reagents such as $FeCl_2.4H_2O$ (%99 Merck), $FeCl_3.6H_2O$ (%99.9 Merck), 3-aminopropyltriethoxysilane (APTES) (%98 Merck), and Itaconic acid (IA) (>99% Merck) were used without further purification. The dye removal process was carried out in deionized water.

2.2. Apparatus

The FT-IR and UV-Vis. spectra were recorded by Thermo Nicolet NEXUS 670 FTIR Fourier transform infrared spectrophotometer (Thermo Scientific, USA) and Agilent 8453 Diode Array UV-Vis. spectrophotometer (Agilent Technologies, USA), respectively. The X-ray diffraction (XRD) patterns were measured on X'Pert Pro X-ray photoelectron spectrometer (Netherlands) using nonmonochromated Cu Kα radiation as an excitation source. The measuring of the magnetic properties of the prepared samples was carried out using a vibrating sample magnetometer (VSM) analysis (Lakeshore Cryotronics, Westerville, OH, USA). The thermogravimetric analysis (TGA) was carried out (Linseis Thermal Analyzer, Germany) at a heating rate of 10°C/min under an N_2 atmosphere. The field emission scanning electron microscopy (FE-SEM) images were obtained from MIRA3 TESCAN (Czech Republic).

2.3. Preparation of MNPs

The preparation of MNPs was carried out using the co-precipitation method [13, 28]. $FeCl_2.4H_2O$ (2.99 g, 15.039 mmol) and $FeCl_3.6H_2O$ (5.41 g, 20.014 mmol) were dissolved in deionized water (50 mL) and the aqueous solution was heated at 80 °C. Then the aqueous solution of ammonium hydroxide (10 mL, 37%) was added to the above-prepared solution along with vigorous stirring at 80°C under an inert atmosphere. The obtained black precipitate was collected by an external magnet, washed several times with deionized water, and finally dried in a vacuum oven at 50°C for 24 hours. The preparation reactions of Fe_3O_4 nanoparticles are presented as follows:

$$Fe^{2+} + 2OH^- \rightarrow Fe(OH)_2$$

$$Fe^{3+} + 3OH^- \rightarrow Fe(OH)_3$$

$$Fe(OH)_2 + Fe(OH)_3 \rightarrow Fe_3O_4 + 4H_2O$$

The overall reaction can be written as:

$$Fe^{2+} + Fe^{3+} + 8(OH)^- \rightarrow Fe_3O_4 + 4H_2O$$

2.4. Modification of MNPs with APTES and AC

In a 100 mL two-necked round-bottom flask equipped with a reflux condenser and inert gas inlet and outlet, absolute ethanol (80 mL) was added and deoxygenated using a capillary tube. Then the MNPs (1.00 g) were added and sonicated for 30 minutes under an inert atmosphere. Finally, APTES (2.00 mL, 8.54 mmol) was added to the flask and sonicated for additional 30 minutes. The mixture was then stirred for 24 hours at 50 °C. The product was separated by an external magnet, washed several times with diethyl ether, and dried at room temperature.

In the next step, into a 100 mL round-bottom flask containing dichloromethane (50 mL) was added MNPs-NH2 (1.00 g). The mixture was degassed along with sonication for 30 minutes. Then the AC (2.68 mL, 33.16mmol) and triethylamine (4.62 mL, 33.16 mmol) was added to the same flask and stirred for 48 h at room temperature under an inert atmosphere. The final product was collected by an external magnet, washed several times with fresh dichloromethane followed by diethyl ether, and dried at room temperature. The overall reaction is shown in **Scheme 1.**

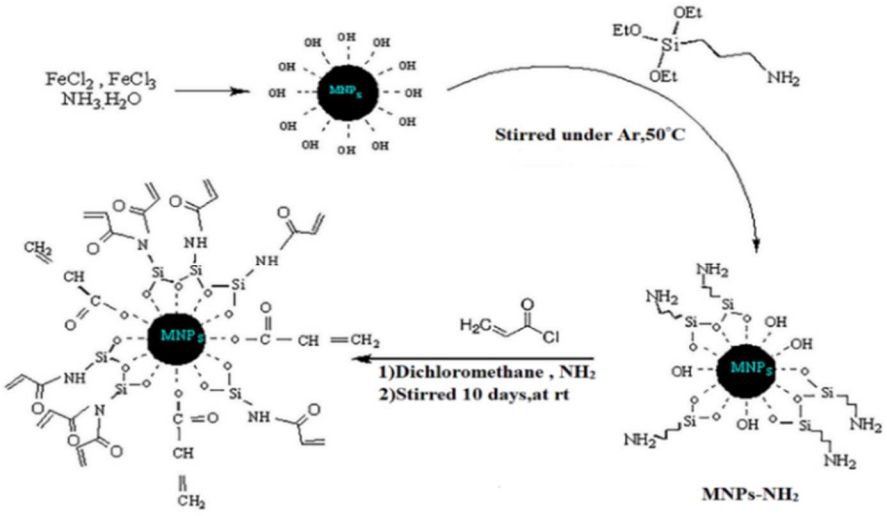

Scheme 1. The overall procedure for the synthesis of the Fe_3O_4@AC.

2.5. Synthesis of the magnetic adsorbent (Fe_3O_4@PHEMAIA)

To synthesize the Fe_3O_4@PHEMAIA, the modified MNPs (1.00 g) were added into a 100 mL two-necked round-bottom flask equipped with a reflux condenser and inert gas inlet and outlet containing THF (40 mL) and sonicated for 30 minutes. Then the IA (2.00 g, 15.37 mmol) and the HEMA (1 g mL, 7.68 mmol) was added to the mixture followed by deoxygenating using a capillary tube. Finally, AIBN (0.056 g, 0.341 mmol) was added and the flask was kept under an inert atmosphere and stirred for 24 hours at 70°C. The final product was separated using an external magnet, washed several times with fresh THF and diethyl ether, and dried at room temperature. The synthesis route is shown in **Scheme 2.**

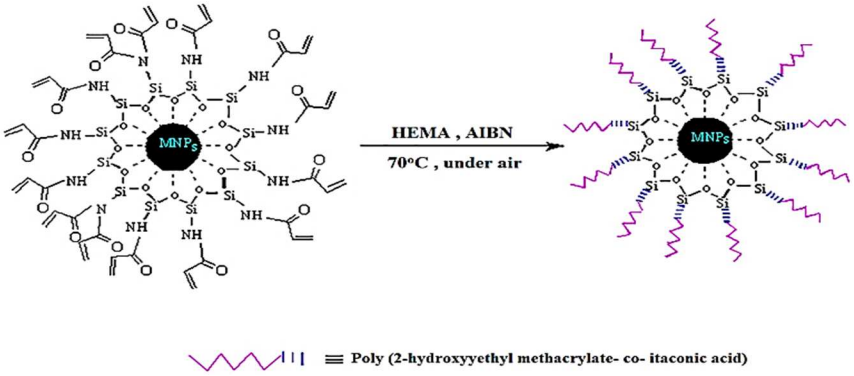

Scheme 2. The schematic presentation of nanocomposite preparation.

2.6. Batch adsorption experiments

The adsorption of MB by the prepared Fe_3O_4@PHEMAIA adsorbent was measured from batch adsorption experiments using 10 mg of the adsorbent in 10 ppm solution of the dye (20 mL) for 60 minutes as predetermined values. The adsorption parameters were then optimized by varying the corresponding parameter in the following order: pH effect, adsorbent amount, initial concentration of the dye, and contact time. Each time the adsorbent was separated by an external magnet and the supernatant was centrifuged for 15 minutes at 3400 rpm, then measured by the UV-Vis spectrophotometer.

3. Results and discussion

3.1. Structural characterization

The FT-IR spectra of the samples were shown in **Figure 1**. In **Figure 1a**, which is related to the bare nanoparticles, the strong absorption peak at 568 cm^{-1} belongs to the stretching vibrations of Fe-O bonds. Besides, the two absorption bands at 3386 and 1623 cm^{-1} are attributed to the stretching and bending vibrations of the surface OH groups, respectively [13]. In spectrum b, in which the nanoparticles have been modified with the APTES, the two peaks at 1022 and 1104 cm^{-1} are related to Si-O-Si bonds and confirm the reaction success. Also, the stretching and bending vibrations of N-H bonds appeared at 3413 and 1550 cm^{-1}, respectively. Moreover, the presence of propyl groups is confirmed by the peak at 2924 cm^{-1}, which is attributed to aliphatic C-H stretching vibrations. In **Figure 1c**, the reaction of the silylated MNPs with the acryloyl chloride has led to appear an absorption band at 1621 cm^{-1}, which is attributed to the amidic carbonyl group. Moreover, the absorption peak at 1712 cm^{-1} is related to esteric carbonyl groups obtained from the reaction of remaining hydroxyl groups with acryloyl chloride. In the final step, copolymerization of the HEMA and the IA on the surface of the modified MNPs has been carried out (**Figure 1d**). In this spectrum, the -COO- groups of the IA and the esteric carbonyl groups of HEMA are shown at 1590 and 1714 cm^{-1}, respectively. Besides, the aliphatic C-H bond absorption peak has been grown at 2933 cm^{-1}, showing the successful polymerization process.

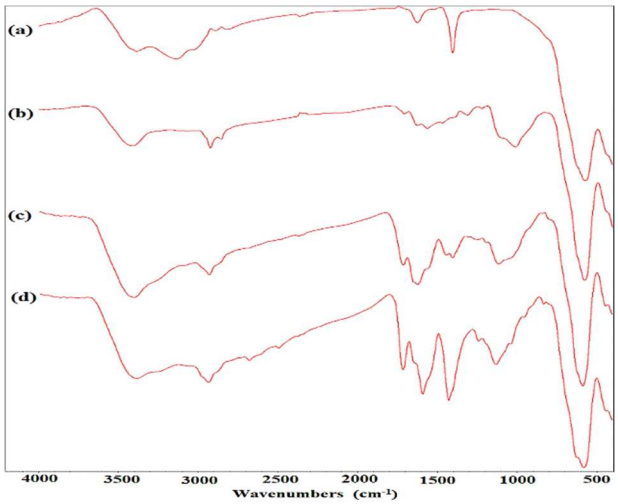

Figure 1. The FT-IR spectrum of the pure Fe_3O_4 **(a)**, the Fe_3O_4 modified with APTES **(b)**, the Fe_3O_4 modified with AC **(c)**, and the Fe_3O_4@PHEMAIA nanocomposite **(d)**.

The crystallinity of the samples is identified by XRD analysis. **Figure 2** shows the XRD patterns of the samples. The intense diffraction peaks at (2θ = 30.27°, 35.63°, 43.29°, 53.64°, 57.14°, 62.73°, and 74.25°), which correspond to the (220), (311), (400), (422), (511), (440), and (533), indicated a cubic spinel structure of the prepared MNPs (**Figure 2a**), which is matched to the standard XRD pattern of the magnetite (JCPDS card, file no. 851436) [29]. These peaks also appeared for the patterns of the acryloyl chloride-modified MNPs and the final adsorbent (patterns b and c), but the baselines have been broadened, showing the successful coating of the amorphous structures of the modifying agent and the copolymer, respectively.

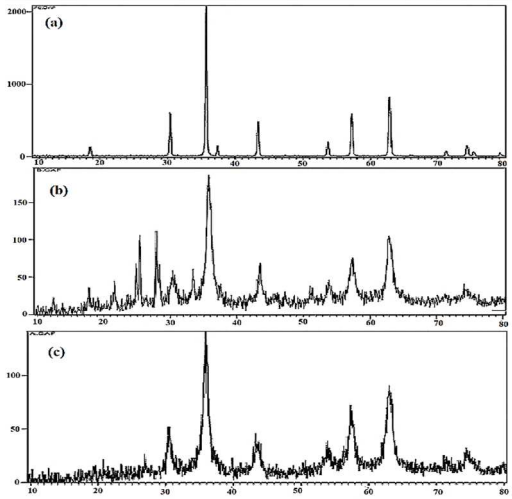

Figure 2. The XRD patterns of the pure magnetite **(a)**, the Fe_3O_4 modified with AC **(b)**, and the Fe_3O_4@PHEMAIA **(c)**.

The magnetic measurements of the samples were studied by VSM at room temperature and the results are shown in **Figure 3**. The magnetic saturation for the naked MNPs (a), the acryloyl chloride-modified MNPs (b), and the Fe_3O_4@PHEMAIA (c) are 80.53, 37.41, and 31.72 emu.g^{-1}, respectively. From these results, it can be concluded that the magnetization decreases by coating non-magnetic species on the MNPs from the modifying agent to the copolymer. This decrease is attributed to the quenching of the magnetic moment by the interplay between the layers and the MNPs surface[29]. However, the magnetic property of the final adsorbent was strong enough to be separated by an external magnet.

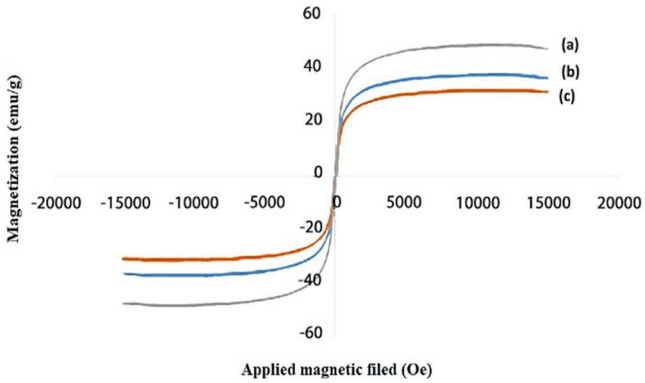

Figure 3. The magnetization curves of the pure Fe_3O_4 **(a)**, the Fe_3O_4 modified with AC **(b)**, and Fe_3O_4@PHEMAIA **(c)**.

Figure 4 shows the TGA thermograms of the final adsorbent. In thermogram a, a slight weight loss from 50 to 200 ^{o}C is due to the loss of moisture[30]. As expected, bare MNPs are thermally stable and do not show any remarkable weight loss up to 800^{o}C. In thermogram b, which is related to the Fe_3O_4@PHEMAIA, a completely different diagram is shown. As can be seen in this thermogram, a three-step degradation is observable. The first degradation step is maybe related to the disjunction of pendant groups such as COO^- and emission of CO and CO_2. The second degradation step starting from 260°C up to about 500°C is attributed to the degradation of small polymeric chains and the final step starting from 540°C is due to the degradation of the remaining long-chain polymers. It should be mentioned that according to the thermogram a, the MNPs are still stable and the remaining weight is attributed to these species.

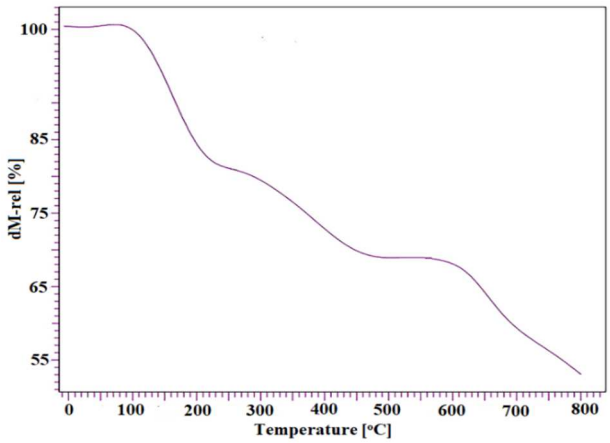

Figure 4. The TGA curve of the Fe_3O_4@PHEMAIA nanocomposite.

The surface morphology of the final sample was investigated using the FE-SEM technique. The images of the Fe_3O_4@PHEMAIA are depicted in **Figure 5**. The image of bare MNPs was investigated in our previous report [13]. As shown in **Figure 5**, the quasi-spherical shape of the MNPs is still observable with an almost attached and aggregated structure, due to the formation of copolymer chains around the particles. The particle size of the Fe_3O_4@PHEMAIA is mainly in the range of 16 to 24 nm.

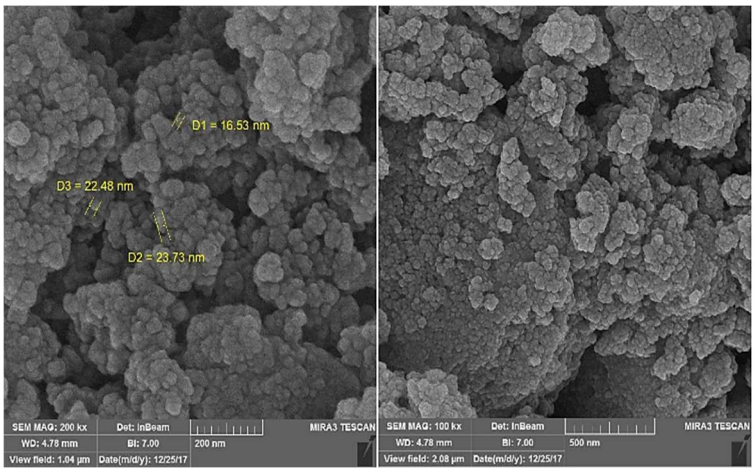

Figure 5. The SEM image of the synthesized nanocomposite.

3.2. Adsorption studies

To calculate the equilibrium adsorption capacity, the following equation (1) was used:

$$q_e=(C_0-C_e)(\frac{V}{m}) \qquad (1)$$

Where q_e is the equilibrium adsorption capacity (mg. g^{-1}), and C_0 and C_e (mg. L^{-1}) are the initial and equilibrium concentrations of the dye, respectively. V (L) is the volume of the solution and m (mg) is the dosage of the adsorbent. The removal percentage of the dye was also calculated using the following equation (2):

$$R(\%)=\frac{(C_0-C_e)}{C_0}\times 100 \qquad (2)$$

3.2.1. The pH effect

Figure 6a shows the effect of the pH value on the adsorption process. As can be seen, the highest adsorption percentage was obtained at pH=11. Higher adsorption percentage at basic pH values may be due to the deprotonation of the adsorption sites and increasing the inclination of the adsorbent to interact with the cationic structure of the dye. The adsorption percentage reached its maximum value at pH=11 and remained constant by increasing more. Therefore, the optimum pH value was selected to be 11.

3.2.2. The adsorbent dosage effect

As shown in **Figure 6b**, which is related to the optimization of the adsorbent dosage, the highest adsorption percentage was obtained with 30 mg of the prepared adsorbent. It is well-known that by increasing the dosage of the adsorbent, the number of adsorption sites increases and leads to an increase in the adsorption percentage; but after the optimized dosage, the adsorption sites start to interact with each other and engage intra-molecular interactions. These interactions lead to a decrease in the number of efficient adsorption sites and subsequently, the adsorption percentage. From this diagram, the optimum dosage was selected to be 30 mg.

3.2.3. The dye initial concentration effect

The results of the initial concentration effect of dye are shown in **Figure 6c**. It can be seen that by increasing the initial concentration of the dye, the adsorption percentage increases and reaches a maximum value, then decreases. This decrease is due to the saturation of the adsorption sites on the adsorbent and the disability of the adsorbent to interact with the dye. Therefore, the maximum initial concentration of the dye in this work was 20 ppm.

3.2.4. The contact time effect

Figure 6d shows the adsorption percentages at different contact times. As shown in this diagram, by increasing the contact time up to 15 minutes, the adsorption percentage increases because the adsorbent and the dye molecules gain enough time to interact with each other. By increasing the contact time by more than 15 minutes, the adsorption percentages show rather constant values, meaning that the contact time is high enough to reach the maximum adsorption; therefore, after this time, no more adsorption happens. Thus, the optimum contact time was selected to be 15 minutes.

Briefly, the optimized values for adsorption parameters are as follows: pH=11, adsorbent dosage=30 mg, initial concentration of the dye=20 ppm, and contact time=15 minutes.

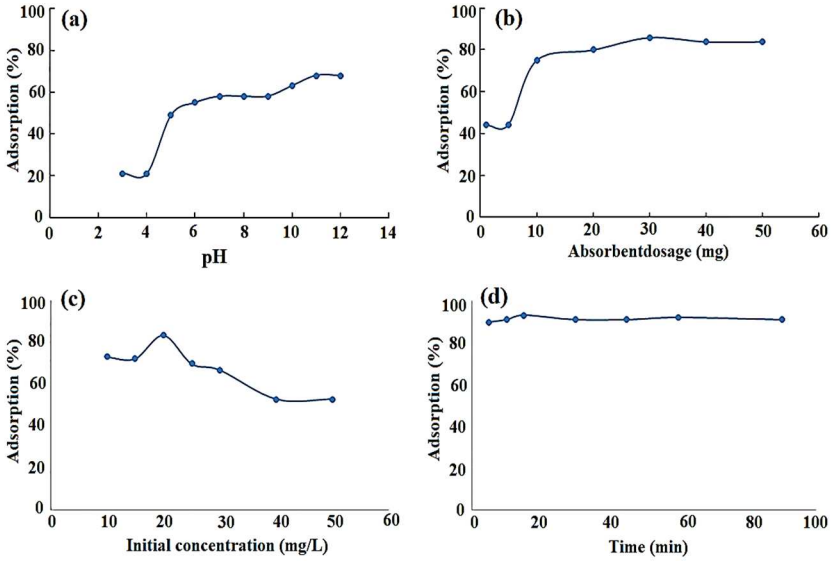

Figure 6. The Effect of pH **(a)**, adsorbent dosage **(b)**, initial concentration **(c),** and adsorption time **(d)** on the MB adsorption by the Fe_3O_4@PHEMAIA nanocomposite.

3.2.5. The study of adsorption isotherms

Adsorption isothermal models were employed to understand the adsorption mechanism of the dye. The adsorption isotherm is one of the most useful parameters to show how the adsorbate molecules are distributed between the liquid phase and the solid phase. In this work, two isothermal models were used to explain the adsorption equilibrium: The Langmuir and Freundlich isotherms; which are briefly described in the following:

The Langmuir model states that adsorption takes place at particular homogeneous sites into the adsorbent surface by monolayers with transmigration of the adsorbed molecules on the plane of the surface [31]. The following equation (3) describes the Langmuir isotherm:

$$q_e=\frac{q_m K_L C_e}{1+K_L C_e} \quad (3)$$

It can be converted to its linear form as follows equation (4):

$$\frac{C_e}{q_e}=\frac{1}{K_L q_m}+\frac{C_e}{q_m} \quad (4)$$

Where q_e ($mg.g^{-1}$) represents the number of the adsorbate molecule, which is adsorbed onto the surface at the equilibrium state; C_e ($mg.L^{-1}$) is the equilibrium concentration of the dye; q_m is the maximum adsorption capacity corresponding to complete monolayer coverage, and K_L ($L.mg^{-1}$) is the Langmuir adsorption equilibrium constant. The q_m and K_L values can be determined from the slope and the y-intercept of the linear plot of C_e/q_e versus C_e, respectively (**Figure 7a**). The R_L factor, which indicates that the type of isotherm is irreversible ($R_L=0$), favorable ($0<R_L<1$), linear ($R_L=1$), or unfavorable ($R_L>1$), and can be determined from the following equation (5) [32] :

$$R_L=\frac{1}{1+K_L C_0} \quad (5)$$

Where C_0 ($mg.L^{-1}$) is the initial concentration of the dye. The values are collected in **Table 1**. The Freundlich isotherm model is to describe multilayer adsorption on a heterogeneous adsorbent surface with a non-uniform distribution of adsorption heat. It is used to evaluation of the adsorption intensity of the adsorbent to the adsorbate and is assumed that the first strong and quick adsorption occurs at binding sites, which depends on the concentration of the adsorbate molecule in the solution. The strength of binding is decreased with the increase of occupied sites [33]. This isotherm is defined by the following equation (6):

$$q_e=K_F C_e^{\frac{1}{n}} \quad (6)$$

The linear form can be expressed as follows in equation (7):

$$\log q_e=\frac{1}{n}\log C_e+\log K_F \quad (7)$$

Where K_F is the Freundlich constant indicating adsorption capacity; and n is an experimental parameter related to the intensity of adsorption. For a favorable adsorption process, the n value should be in the range of 1-10. The n and K_F can be calculated from the slope and y-intercept of the linear plot of log q_e versus log C_e, respectively (**Figure 7b**). All data of the adsorption isotherm study are summarized in **Table 1**. From this table and related R^2 values, it can be concluded that the Langmuir isotherm fitted to the experimental data more than the Freundlich model. Moreover, the E value shows that the type of adsorption in this work is Langmuir.

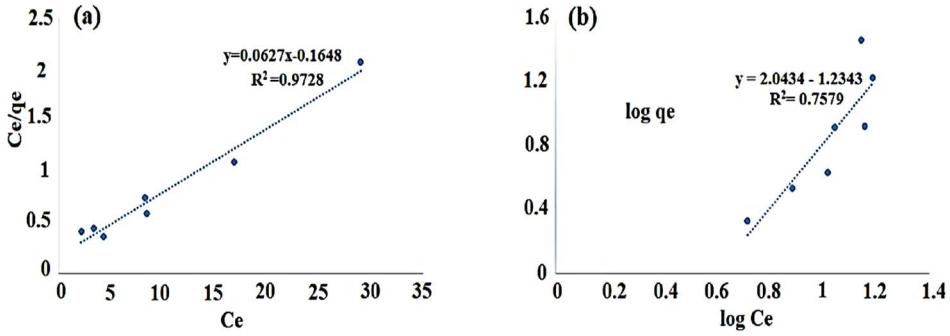

Figure 7. The Langmuir **(a)**, and the Freundlich **(b)** adsorption isotherms for the MB adsorption onto the Fe_3O_4@PHEMAIA nanocomposite.

Table 1. Parameters of isotherm models for the adsorption of MB by the adsorbent

Isotherm	Parameters	MB
Langmuir	q_m (mg g^{-1})	16.129
	K_L(L mg^{-1})	0.49679
	R_L	0.09141
	R^2	0.9728
Freundlich	K_F (mg g^{-1})	0.0583
	N	0.489
	R^2	0.7579

3.2.6. The study of adsorption kinetics

To study the adsorption kinetics and discuss the adsorption mechanism rate of the dye onto the prepared magnetic nanocomposite, two kinetic models were employed to fit the experimental data: The Lagergren pseudo-first-order and the Ho pseudo-second-order equations [34]. The Lagergren kinetic model discusses the adsorption proportional rate to the number of unoccupied sites by solutes and indicates by the following linear equation (8):

$$\log(q_e-q_t)=-\frac{K_1}{2.0303}t+\log q_e \qquad (8)$$

Where q_t and q_e ($mg.g^{-1}$) are the number of adsorbed dye molecules at the time *t* (min) and the equilibrium state, respectively. K_1 (min^{-1}) is the pseudo-first-order adsorption kinetic constant. Both K_1 and q_e can be achieved from the slope and y-intercept of $\log(q_e-q_t)$ versus *t* (**Figure 8a**). The Ho kinetic model is based on the adsorption equilibrium capacity and supposes that the ownership rate for adsorption sites is proportional to the square of unoccupied sites number. The rate of adsorption is based on the activated sites' concentration on the surface of the adsorbent. This model is indicated by the following equation (9):

$$\frac{t}{q_e}=\frac{1}{K_2q_e^2}+\frac{1}{q_e}t \qquad (9)$$

Where K_2 ($g.mg^{-1}.min^{-1}$) is the pseudo-second-order adsorption kinetic parameter. The K_2 and q_e can be achieved from the y-intercept and slope of the graph of (t/q_t) versus t (**Figure 8b**). The experimental data of the two mentioned kinetic models are calculated and summarized in **Table 2**. According to the R^2 values from this table, it is obvious that the kinetic model is fitted to the pseudo-second-order model.

Moreover, the values of normalized standard deviation (NSD%) were calculated to confirm the fitness of the experimental data to the kinetic models. The NSD% equation is expressed as follows equation (10):

$$NSD\% = \frac{\sqrt{\sum[(q_{e,exp}-q_{e,cal})/q_{e,exp}]^2}}{N-1} \quad (10)$$

Where N is related to the number of measurements, $q_{e,exp}$, and $q_{e,cal}$ ($mg.g^{-1}$) are the experimental and calculated adsorption capacities at the equilibrium state, respectively. From the NSD% values shown in **Table 2**, it is also clear that the Ho model is more fitted with the experimental data, because of the lower NSD% value.

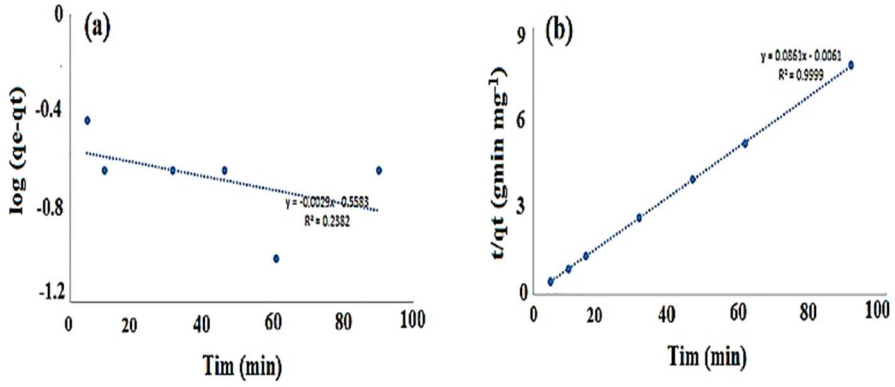

Figure 8. The Kinetic models of the MB adsorption onto the Fe_3O_4@PHEMAIA nanocomposite using pseudo-first-order **(a)**, and pseudo-second-order model **(b)**.

Table 2. Parameters of kinetic models for the adsorption of MB adsorption

Kinetic models and parameters	MB
Pseudo-first-order model	
$q_{e,exp}$ (mg g^{-1})	11.826
$q_{e,cal}$ (mg g^{-1})	0.28
K_1(min^{-1})	0.0067
R^2	0.2382
NSD (%)	0.32
Pseudo-second-order model	
$q_{e,exp}$ (mg g^{-1})	11.826
$q_{e,cal}$ (mg g^{-1})	1.16
K_2	121.81
R^2	0.9999
NSD (%)	0.407

4. Conclusion

In this work, a magnetic nanocomposite was successfully synthesized via modification of Fe_3O_4 nanoparticles to remove the methylene blue as a typical dye from aqueous solutions. Different adsorption parameters such as pH, adsorbent amount, dye initial concentration, and contact time were investigated and optimized. The results showed that the nanocomposite has adsorption efficiency toward the methylene blue dye within 15 minutes in pH=11, adsorbent dosage=30 mg, and with an initial concentration of the dye=20 ppm. The result of VSM showed that the obtained nanocomposite has a magnetic property, which eases its separation and its amount, which is 31.72 emu. g^{-1}. Finally, the obtained nanocomposite has the ability in removing the selected dye by more than 89%. Moreover, the adsorption isotherms and kinetics were studied to determine the adsorption mechanism and the results showed that

the Langmuir isotherm best fitted to the experimental than the Freundlich model. It is also found that the Ho model is more fitted with the experimental data.

Authors' contributions

All authors contributed to data analysis, drafting and revising of the paper and agreed to be responsible for all the aspects of this work.

Acknowledgments

The authors wish to acknowledge financial and spiritual support from Urmia University.

Declaration of competing interest

The authors declare no competing interest.

Funding

This paper received no external funding.

Data availability

Data will be made available on request.

References

[1] Q. Wu, Ch. Feng, Ch. Wang, Zh. Wang, A facile one-pot solvothermal method to produce superparamagnetic graphene–Fe_3O_4 nanocomposite and its application in the removal of dye from aqueous solution, Colloids Surf. B. 101 (2013) 210-214.
[2] G. Crini, Non-conventional low-cost adsorbents for dye removal: A review, Bioresour. Technol. 97 (2006) 1061-1085.
[3] Z. Zhang, j. Kong, Novel magnetic Fe_3O_4@C nanoparticles as adsorbents for removal of organic dyes from aqueous solution, J. Hazard. Mater. 193 (2011) 325-329.
[4] S. Qu, F. Huang, S. Yu, G. Chen, J. Kong, Magnetic removal of dyes from aqueous solution using multi-walled carbon nanotubes filled with Fe_2O_3 particles, J. Hazard. Mater. 160 (2008) 643-647.
[5] M. Kornaros, G. Lyberatos, Biological treatment of wastewaters from a dye manufacturing company using a trickling filter, J. Hazard. Mater. 136 (2006) 95-102.
[6] E. Guibal, J. Roussy, Coagulation and flocculation of dye-containing solutions using a biopolymer (Chitosan), React. Funct. Polym. 67 (2007) 33-42.
[7] W. Zhao, Z. Wu, Wang, D, Ozone direct oxidation kinetics of Cationic Red X-GRL in aqueous solution, J. Hazard. Mater. 137 (2006) 1859-1865.
[8] K. Dutta, S. Mukhopadhyay, S. Bhattacharjee, B. Chaudhuri, Chemical oxidation of methylene blue using a Fenton-like reaction, J. Hazard. Mater. 84 (2001) 57-71.
[9] G. Capar, U. Yetis, L. Yilmaz, Membrane-based strategies for the pre-treatment of acid dye bath wastewaters, J. Hazard. Mater. 135 (2006) 423-430.
[10] C.H. Liu, J.S. Wu, H.C. Chiu, S.Y. Suen, K.H. Chu, Removal of anionic reactive dyes from water using anion exchange membranes as adsorbers, Water Res. 41 (2007) 1491-1500.
[11] M. Muruganandham, M. Swaminathan, TiO_2–UV photocatalytic oxidation of Reactive Yellow 14: Effect of operational parameters, J. Hazard. Mater. 135 (2006)78-86.
[12] R. De Lisi, G. Lazzara, S. Milioto, N. Muratore, Adsorption of a dye on clay and sand. Use of cyclodextrins as solubility-enhancement agents, Chemosphere. 69 (2007) 1703-12.
[13] S. Ehsanimehr, P. N. Moghadam,W.Dehaen, V. Shafiei- Irannejad, PEI grafted Fe_3O_4@SiO2@SBA-15 labeled FA as a pH-sensitive mesoporous magnetic and biocompatible nanocarrier for targeted delivery of doxorubicin to MCF-7 cell line, Colloids Surf. A Physicochem. Eng. 615 (2021) 126302.
[14] M. Rafatullah, O. Sulaiman, R. Hashim, A. Ahmad, Adsorption of methylene blue on low-cost adsorbents: A review, J. Hazard. Mater. 177 (2010) 70-80.
[15] H. Zhu, R. Jiang, J. Li, Y. Fu, S. Jiang, J. Yao, Magnetically recyclable Fe_3O_4/Bi2S3 microspheres for effective removal of Congo red dye by simultaneous adsorption and photocatalytic regeneration, Sep. Purif. Technol. 179 (2017) 184-193.
[16] M.A. Salam, R.M. El-Shishtawy, A.Y. Obaid, Synthesis of magnetic multi-walled carbon nanotubes/magnetite/chitin magnetic nanocomposite for the removal of Rose Bengal from real and model solution, J. Ind. Eng. Chem. 20 (2014) 3559-3567.
[17] R. Jiang, J. Yao, H. Zhu, Y. Fu, Y. Guan, L. Xiao, G. Zeng Effective decolorization of congo red in aqueous solution by adsorption and photocatalysis using novel magnetic alginate/γ-Fe_2O_3/CdS nanocomposite, Desalination and Water Treatment, 52 (2014) 1-3.

[18] H.Y. Zhu, R. Jiang, L. Xiao, W. Li, A novel magnetically separable γ-Fe_2O_3/crosslinked chitosan adsorbent: Preparation, characterization and adsorption application for removal of hazardous azo dye, J. Hazard. Mater. 179 (2010) 251-257.
[19] C.T. Yavuz, J.T. Mayo, W.Y. William, A. Prakash, J.C. Falkner, S. Yean, L. Cong, H.J. Shipley, A. Kan, M. Tomson, Low-field magnetic separation of monodisperse Fe_3O_4 nanocrystals, Natelson, science. 314 (2006) 964-7.
[20] H.Y. Zhu, R. Jiang, S.H. Huang, J. Yao, F.Q. Fu, J.B. Li, Novel magnetic $NiFe_2O_4$/multi-walled carbon nanotubes hybrids: Facile synthesis, characterization, and application to the treatment of dyeing wastewater, Ceramics Int.41(2015) 11625-11631.
[21] R. Jiang, H.Y. Zhu, J.B. Li, F.Q. Fu, J. Yao, S.T. Jiang, G.M. Zeng, Fabrication of novel magnetically separable BiOBr/CoFe2O4 microspheres and its application in the efficient removal of dye from aqueous phase by an environment-friendly and economical approach, Applied Surface Sci. 364 (2016) 604-612.
[22] S. Shukla, R. Khan, A. Daverey, Synthesis and characterization of magnetic nanoparticles, and their applications in wastewater treatment: A review, Environ. Technol. Innov. 24, (2021) 101924.
[23] S.H. Araghi, M.H. Entezari, M. Chamsaz, Modification of mesoporous silica magnetite nanoparticles by 3-aminopropyltriethoxysilane for the removal of Cr(VI) from aqueous solution, Microporous Mesoporous Mater. 218 (2015) 101-111.
[24] D. Horák, M. Trchová, M.J. Beneš, M. Veverka, Monodisperse magnetic composite poly (glycidyl methacrylate)/La0.75Sr0.25MnO3 microspheres by the dispersion polymerization, E. Pollert, Polymer. 51 (2010) 3116-3122.
[25] D. Ghosh, K.G. Bhattacharyya, Adsorption of methylene blue on kaolinite, Appl Clay Sci. 20 (2002) 295-300.
[26] J. Fu, Z. Chen, M. Wang, S. Liu, J. Zhang, J. Zhang, R. Han, Q. Xu, Adsorption of methylene blue by a high-efficiency adsorbent (polydopamine microspheres): Kinetics, isotherm, thermodynamics and mechanism analysis, Chem. Eng. J. 259 (2015) 53-61.
[27] L. Y. Yee,Q. H. Ng,S.H. Shuit,S.K . Enche ,D.M. Nawi,S. Chun Low, Application of the novel pH-catalytic-magnetic tri-functionalities augmented bead for removal of organic dye pollutants, Environ Prog Sustainable Energy. (2021) e13699.
[28] D. Maity, D.C. Agrawal, Synthesis of iron oxide nanoparticles under oxidizing environment and their stabilization in aqueous and non-aqueous media, J. Magn. Magn. Mater. 308 (2007) 46-55.
[29] J. Liu, W. Wang, H. Liu, Y. Zhou, H. Zhang, X. Zhou, Penicillium expansum lipase-coated magnetic Fe_3O_4–polymer hybrid hollow nanoparticles: a highly recoverable and magnetically separable catalyst for the synthesis of 1,3-dibutylurea, RSC Adv. 4 (2014) 25983-25992.
[30] M. Ozmen, K. Can, G. Arslan, A. Tor, Y. Cengeloglu, M. Ersoz, Adsorption of Cu (II) from aqueous solution by using modified Fe_3O_4 magnetic nanoparticles, Desalination. 254 (2010) 162-169.
[31] Y.M. Hao, C. Man, Z.B. Hu, Effective removal of Cu (II) ions from aqueous solution by amino-functionalized magnetic nanoparticles, J Hazard Mater. 184 (2010) 392-399.
[32] K.R. Hall, L.C. Eagleton, A. Acrivos, T. Vermeulen, Pore and Solid Diffusion Kinetics in Fixed Bed Adsorption under Constant Pattern Conditions, Ind. Eng. Chem. Fundam. 5 (1966) 212-223.
[33] R.M. Ali, H.A. Hamad, M.M. Hussein, G.F. Malash, Potential of using green adsorbent of heavy metal removal from aqueous solutions: Adsorption kinetics, isotherm, thermodynamic, mechanism and economic analysis, Ecol. Eng. 91 (2016) 317-332.
[34] P.A. Alaba, N.A. Oladoja, Y.M. Sani, O.B. Ayodele, I.Y. Mohammed, S.F. Olupinla, W.M.W. Daud, Insight into wastewater decontamination using polymeric adsorbents, J Environ Chem Eng. 6 (2018) 1651.